J Mater Sci (2010) 45:5637–5641
DOI 10.1007/s10853-010-4628-8

Study on crystallization behavior and microstructure of melt-spun $Nd_2(Fe,Nb)_{14}B/\alpha$-Fe alloys

C. Wang · M. Y. Lan · M. Yan

Received: 19 January 2010 / Accepted: 17 May 2010 / Published online: 4 June 2010
© Springer Science+Business Media, LLC 2010

Abstract The effects of Nb addition on the crystallization behavior, microstructure, and magnetic properties of melt-spun $Nd_2Fe_{14}B/\alpha$-Fe nanocomposite magnets have been studied. The addition of Nb can significantly improve the thermal stability of amorphous phase in as-spun alloys, narrow the range between the onset crystallization temperature and the optimal annealing temperature, restrain the initial formation and growth of α-Fe and $Nd_2Fe_{14}B$. A finer and more homogeneous microstructure can be obtained in the Nb-doped alloy than in the Nb-free alloy. And the Nb addition makes the grains more equiaxed shape. The $Nd_{10}Fe_{83}Nb_1B_6$ alloy annealed at 715 °C for 10 min exhibits the improved magnetic properties, $B_r = 0.90$ T, ${}_iH_c = 750$ kA/m, $(BH)_{max} = 120$ kJ/m^3, the intrinsic coercivity and the maximum energy product increase by 25% and 14%, compared with the $Nd_{10}Fe_{84}B_6$ alloy.

Introduction

Nanocomposite magnetic materials consisting of a hard magnetic phase exchange coupled to a soft magnetic phase have attracted considerable attention due to their high remanence ratio, high energy product, and low rare-earth content. The high permanent magnetic properties depend on both the excellent intrinsic magnetic properties and the microstructure of the materials. For the effective exchange coupling, a homogeneous and fine-grained microstructure is required.

Microalloying is an effective way to improve the magnetic properties by optimizing the microstructure and improving the intrinsic magnetic properties of magnetic phases [1–5]. Addition of Nb was reported to be advantageous in improving the energy product of nanocomposite magnets due to a refinement in microstructure [6–8]. On the other hand, Jin et al. [9] reported that some large grain clusters were observed in Nb-doped alloy, thus degrading the squareness of hysteresis loops and decreasing the energy product. Ping et al. [10] reported that the Nb-doped ribbons prepared by annealing amorphous precursors exhibit coarser microstructures than the Nb-free ribbons prepared by melt spinning at a roll speed of 20 m/s. So, the effects of Nb in nanocomposite magnets need to be further studied.

At present, over quenching the alloy (melt spinning at high roll speeds to form amorphous phase in the as-spun ribbons) and then crystallizing the amorphous phase by an appropriate annealing is a usual way to prepare nanocomposite magnets. The crystallization behavior of the alloy plays a key role in the microstructure development. Heretofore, the influences of Nb addition on the crystallization behavior of the $Nd_2Fe_{14}B/\alpha$-Fe magnets have not been understood very well. Our previous study [11] showed that the crystallization behavior of the amorphous Nd–Fe–B alloy changes from a two-step process to a single-step process with the addition of Zr, thus refining the microstructure and improving the magnetic properties of magnets. Nb is adjacent to Zr in the periodic table of elements. It is interesting, then, to ask whether or not the

C. Wang (✉) · M. Y. Lan
College of Materials Science and Engineering,
Fuzhou University, Shangjie Town, Fuzhou 350108,
Fujian Province, China
e-mail: msewang@fzu.edu.cn

M. Yan
State Key Laboratory of Silicon Materials, Zhejiang University,
Hangzhou 310027, China

Nb addition has similar effect in the $Nd_2Fe_{14}B/\alpha$-Fe magnets. In this paper, the effects of Nb addition on the crystallization behavior, microstructure, and magnetic properties of $Nd_2Fe_{14}B/\alpha$-Fe magnets are investigated.

Experiment

Alloy ingots with nominal compositions of $Nd_{10}Fe_{84}B_6$, $Nd_{10}Fe_{83}Nb_1B_6$, $Nd_{10}Fe_{82.5}Nb_{1.5}B_6$, and $Nd_{10}Fe_{82}Nb_2B_6$ were prepared by induction melting under purified argon. Alloy ribbons were obtained by melt spinning in an Ar atmosphere at a roll speed of 35 m/s, and then annealed between 650 and 750 °C for 10 min under vacuum. The magnetic properties were measured using a LakeShore 7410 vibrating sample magnetometer (VSM) with a maximum magnetic field of 2.5 T. Thermomagnetic analysis (TMA) was used to determine the magnetic phases and the corresponding Curie temperatures (T_C). A magnetic field of 0.05 T was applied during the TMA measurement. The crystallization behaviors of as-spun ribbons were traced using a SDT Q600 differential scanning calorimeter (DSC) at a heating rate of 10 °C/min. X-ray diffraction (XRD, Rigaku D/max 2550Pc) with Cu K_α radiation was used to identify the phase composition of samples. The microstructures of samples were observed by a Philips CM200 transmission electron microscope (TEM). The TEM specimens were prepared by ion-milling the ribbons from both sides.

Results and discussion

Figure 1 shows the dependence of the remanence, B_r, the intrinsic coercivity, ${}_iH_c$, and the maximum magnetic energy product $(BH)_{max}$ on the annealing temperature for the $Nd_{10}Fe_{84-x}Nb_xB_6$ ($x = 0$–2) ribbons after annealing for 10 min. It can be seen that, at the same annealing temperature, the intrinsic coercivity increases and the remanence decreases with increasing Nb content. The maximum magnetic energy product first increases as the content of Nb increases, reaches maximum value at $x = 1$, and then decreases with the further increase of Nb content. In this article, the $Nd_{10}Fe_{84}B_6$ and $Nd_{10}Fe_{83}Nb_1B_6$ alloys are selected to study the effects of Nb addition. For $Nd_{10}Fe_{84}B_6$ and $Nd_{10}Fe_{83}Nb_1B_6$ alloys, the magnetic properties (B_r, ${}_iH_c$, and $(BH)_{max}$) first increase with increasing temperature, reach maximum values at the optimum temperature 715 °C, then decrease with the further increase in annealing temperature. The $Nd_{10}Fe_{83}Nb_1B_6$ alloy exhibits the optimal magnetic properties with ${}_iH_c = 750$ kA/m, $B_r = 0.90$ T, and $(BH)_{max} = 120$ kJ/m^3 as compared to 600 kA/m, 0.92 T, and 105 kJ/m^3 for $Nd_{10}Fe_{84}B_6$ alloy.

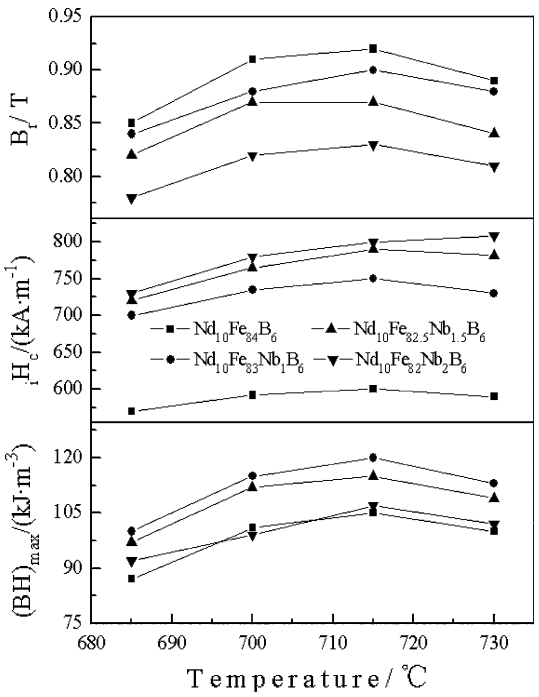

Fig. 1 The remanence, B_r, the intrinsic coercivity, ${}_iH_c$, and the maximum magnetic energy product $(BH)_{max}$ of $Nd_{10}Fe_{84-x}Nb_xB_6$ ($x = 0$–2) ribbons annealed at various temperatures for 10 min

Figure 2 presents the XRD patterns of $Nd_{10}Fe_{84}B_6$ and $Nd_{10}Fe_{83}Nb_1B_6$ alloys. It is shown that, for both alloys, the phase composition transforms from an as-spun amorphous state to a mixture of $Nd_2Fe_{14}B$ and α-Fe phases after optimal annealing. Bright-field TEM images with selected area electron diffraction (SAED) patterns of both the optimally annealed samples are shown in Fig. 3.

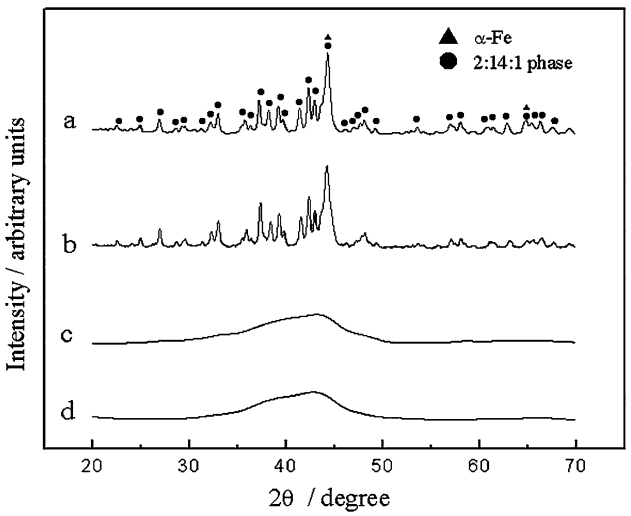

Fig. 2 X-ray diffraction patterns of $Nd_{10}Fe_{84}B_6$ and $Nd_{10}Fe_{83}Nb_1B_6$ ribbons melt-spun at 35 m/s: (*a*) $Nd_{10}Fe_{84}B_6$, optimally annealed; (*b*) $Nd_{10}Fe_{83}Nb_1B_6$, optimally annealed; (*c*) $Nd_{10}Fe_{84}B_6$, without annealing; (*d*) $Nd_{10}Fe_{83}Nb_1B_6$, without annealing

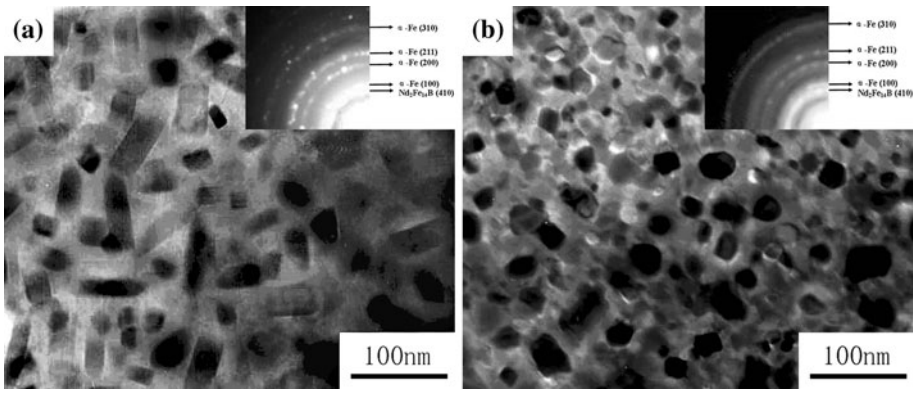

Fig. 3 TEM bright-field images and selected area diffraction patterns of optimally annealed **a** $Nd_{10}Fe_{84}B_6$ and **b** $Nd_{10}Fe_{83}Nb_1B_6$ ribbons

The SAED patterns show that the microstructures of both alloys are crystallographically isotropic, and the rings in SAED patterns can be indexed with those arising from the $Nd_2Fe_{14}B$ and α-Fe phases. Figure 3a indicates that the $Nd_{10}Fe_{84}B_6$ has a heterogeneous microstructure consisting of large $Nd_2Fe_{14}B$ and α-Fe grains, and abnormally coarse grains with grain sizes of ~70 nm can be observed. A significant reduction in grain size with an improvement in microstructural homogeneity is observed in the Nb-doped alloy, as shown in Fig. 3b, although this alloy still contains a few large grains, ~50 nm. So the exchange coupling between the hard and soft magnetic phases is strengthened and the magnetic properties are improved. In addition, one may note that the Nb addition optimizes the shape of grains, making the grains more equiaxed shape. It was reported [12] that a large stray field originating from the sharp edges of grains can reduce the coercivity. Thus, a microstructure with more spherical shaped grains is helpful to improve the coercivity in the Nb-doped alloy. On the other hand, the non-magnetic Nb element would lead to the dilution of the overall magnetization, which may be the reason for the decrease in the remanence of the Nb-doped alloy.

Figure 4 shows the DSC curves for the crystallization of amorphous $Nd_{10}Fe_{84}B_6$ and $Nd_{10}Fe_{83}Nb_1B_6$ alloys. There are two exothermic peaks in both crystallization curves, which mean the crystallization behavior is a two-step process for both alloys. But the second peak for Nb-doped sample is smaller than the corresponding peak for Nb-free sample. By measuring the DSC curves, the latent heat of the second exothermic peak for Nb-free and Nb-doped samples are 4.5 ± 0.2 and 2.7 ± 0.2 J/g, respectively. In order to study further the phase transformation process corresponding to the DSC thermal features, isothermal annealing experiments were carried out on both the as-spun ribbons at different temperatures, and thermomagnetic analysis (TMA) was conducted. XRD was also used to determine the phase composition in the annealed ribbons, but the results are not conclusive enough. Since the XRD patterns of phases in the Nd–Fe–B system, such as

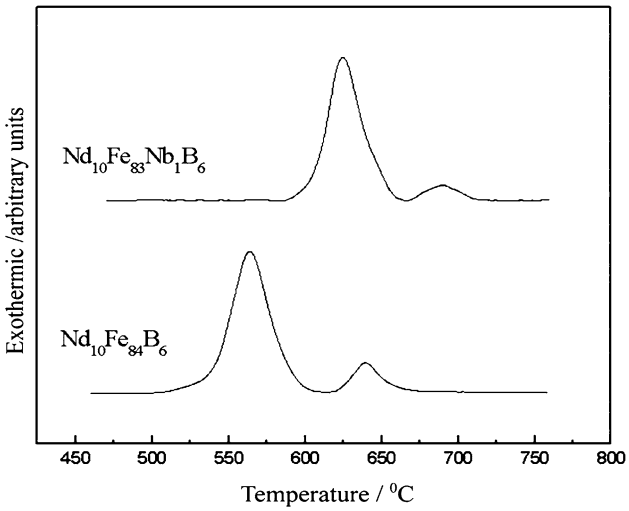

Fig. 4 DSC traces for $Nd_{10}Fe_{84}B_6$ and $Nd_{10}Fe_{83}Nb_1B_6$ ribbons melt-spun at 35 m/s

$Nd_3Fe_{62}B_{14}$, $Nd_2Fe_{23}B_3$, and $Nd_2Fe_{14}B$, are very similar, but the Curie temperatures of all these phases are clearly different [13]. TMA is very useful to investigate the phase composition in these ribbons.

Figure 5 presents the TMA traces for the as-spun $Nd_{10}Fe_{84}B_6$ and $Nd_{10}Fe_{83}Nb_1B_6$ ribbons after isothermal annealing at different temperatures for 3 min. There are the $Nd_3Fe_{62}B_{14}$ metastable phase (T_C = 210 °C [13]), $Nd_2Fe_{14}B$ phase, and α-Fe phase in the $Nd_{10}Fe_{84}B_6$ sample after annealing at 570 °C. The same phases also appear in the $Nd_{10}Fe_{83}Nb_1B_6$ sample after annealing at 625 °C. The $Nd_3Fe_{62}B_{14}$ metastable phase transforms to $Nd_2Fe_{14}B$ and α-Fe phases in both samples after annealing at 715 °C. Thus, for the Nb-free and Nb-doped samples, the first exothermic peak can be attributed to the formation of α-Fe phase, $Nd_2Fe_{14}B$ phase, and $Nd_3Fe_{62}B_{14}$ metastable phase from the amorphous phase, and the second one is related to the transformation from the $Nd_3Fe_{62}B_{14}$ metastable phase to the $Nd_2Fe_{14}B$ and α-Fe phases. Similarly, Hadjipanayis et al. [14] reported the appearance and decomposition of the $Nd_3Fe_{62}B_{14}$ metastable phase in $Nd_6Fe_{87}Nb_1B_6$ alloy.

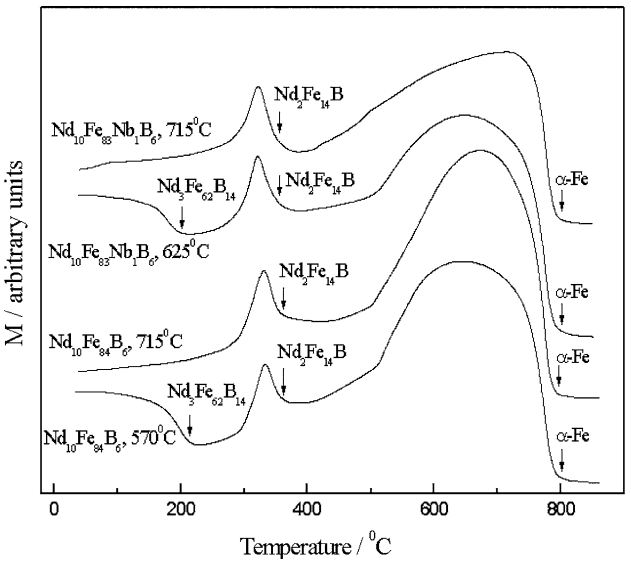

Fig. 5 TMA traces for $Nd_{10}Fe_{84}B_6$ and $Nd_{10}Fe_{83}Nb_1B_6$ ribbons annealed at various temperatures

However, they only observed α-Fe phase and $Nd_3Fe_{62}B_{14}$ metastable phase in the $Nd_6Fe_{87}Nb_1B_6$ ribbons annealed at the temperature of the first exothermic peak. These different observations may be due to the different Nd content between the present work and the previous work. The Nd content is higher in present work which would promote the formation of $Nd_2Fe_{14}B$ phase in the first exothermic peak.

Based on the results of XRD, DSC, and TMA, the $Nd_{10}Fe_{84}B_6$ and $Nd_{10}Fe_{83}Nb_1B_6$ alloys have the same crystallization sequence during annealing. But the addition of Nb significantly improves the thermal stability of the amorphous phase. The onset crystallization temperature of the amorphous phase increases from 500 °C for the $Nd_{10}Fe_{84}B_6$ alloy to 587 °C for the $Nd_{10}Fe_{83}Nb_1B_6$ alloy. For the Nb-free alloy, the range between the optimal annealing temperature 715 °C and the onset crystallization temperature 500 °C is rather large. Thus, the α-Fe and $Nd_2Fe_{14}B$ grains formed early in the first-step crystallization process would be easy to grow coarse during the annealing process. For the Nb-doped alloy, the range between the optimal annealing temperature and the onset crystallization temperature is smaller than that of the Nb-free alloy, which is helpful to restrain the growth of early-formed α-Fe and $Nd_2Fe_{14}B$ grains during the annealing process.

The factors which can influence the thermal stability of amorphous phase are diverse. A possible explanation for the present observation could be the decrease of atomic diffusivity on substituting Nb for Fe, leading to higher crystallization temperature. The crystallization process of amorphous phase is strongly affected by the atomic diffusion. Due to the large atomic diameter, the diffusivity of Nb atoms is low. Moreover, after Nb addition there are more elements and atom radius (of which, Nd > Nb > Fe > B) variety in the as-spun ribbons. Thus, the packing density of atoms would be enhanced, which also inhibits the atomic diffusion. So, the Nb-doped amorphous phase would be expected to have a higher thermal stability than the Nb-free counterpart.

Pervious studies [7, 15] reported that Nb has very low solubility in both the α-Fe and $Nd_2Fe_{14}B$ phases. As shown using three-dimensional atom probe (3DAP) and nano-probe energy dispersive spectroscopy, the Nb tends to enrich the interface between the α-Fe and $Nd_2Fe_{14}B$ grains. In the present work, as shown by the TMA traces, the Curie temperature of $Nd_2Fe_{14}B$ phase decreases a little after Nb addition, and the Curie temperature of α-Fe phase keeps the same in Nb-free and Nb-doped alloys. The Curie temperatures of the $Nd_2Fe_{14}B$ and α-Fe phases are dominated primarily by the exchange interaction between Fe atoms [16–18]. If the additive elements are dissolved in the two phases, the strength of exchange interaction between Fe atoms would be changed, thus leading to the change of the Curie temperatures of the $Nd_2Fe_{14}B$ and α-Fe phases. The TMA result implies that the Nb is hardly dissolved in the α-Fe phase and a fraction of the Nb atoms could be dissolved in the 2:14:1 phase, which agrees with the previous works. The segregation of Nb to the interfaces, in combination with the low atomic diffusion, could reduce the mobility of the interfaces, thus the $Nd_{10}Fe_{83}Nb_1B_6$ alloy has a finer and more equiaxed grain structure than the $Nd_{10}Fe_{84}B_6$ counterpart.

However, the addition of Nb does not change the two-step crystallization process of amorphous phase. In the Nb-doped alloy, some α-Fe and $Nd_2Fe_{14}B$ grains precipitated earlier from the amorphous matrix in the first-step crystallization process still tend to grow larger during the decomposition of metastable phase. It is one of the reasons why the Nb-doped alloy still contains some large grains in the present work and in the previous works [9, 10]. Some Nb atoms may enter the metastable phase, leading to the difference in the latent heat of the second exothermic peak between the two alloys, 4.5 ± 0.2 J/g for $Nd_{10}Fe_{84}B_6$ and 2.7 ± 0.2 J/g for $Nd_{10}Fe_{83}Nb_1B_6$. Therefore, further investigations are needed.

Conclusions

For both $Nd_{10}Fe_{84}B_6$ and $Nd_{10}Fe_{83}Nb_1B_6$ alloys, the crystallization behavior is a two-step process. The addition of Nb significantly improves the thermal stability of amorphous phase, narrows the range between the onset crystallization temperature and the optimal annealing temperature, thus retarding the initial formation and growth of α-Fe and

$Nd_2Fe_{14}B$. A finer and more homogeneous microstructure can be obtained in the Nb-doped alloy. And the Nb addition makes the grains more equiaxed in shape. After optimal annealing, the intrinsic coercivity and the maximum energy product increase from 600 kA/m, 105 kJ/m^3 for $Nd_{10}Fe_{84}B_6$ alloy to 750 kA/m, 120 kJ/m^3 for $Nd_{10}Fe_{83}Nb_1B_6$ alloy, respectively.

Acknowledgements This work is financially supported by the Natural Science Foundation of Fujian Province of China (Grant No.E0710005), the Science and Technology Foundation of Fuzhou University (Grant No.2007-XY-01) and the Elitist Foundation of Fuzhou University (Grant No. 0626).

References

1. Chang HW, Cheng YT, Chang CW, Hsieh CC, Guo ZH, Chang WC, Sun AC (2009) J Appl Phys 105:07A742-1
2. Yang B, Shen BG, Zhao TY, Sun JR (2008) J Magn Magn Mater 320:2406
3. Spyra M, Leonowicz M (2008) J Magn Magn Mater 320:e46
4. Hoque SM, Hakim MA, Khan FA, Dan NH (2007) J Mater Sci 42:9415. doi:10.1007/s10853-007-1884-3
5. Sorescu M, Diamandescu L, Valeanu M, Jianu A (2004) J Mater Sci 39:7387. doi:10.1023/B:JMSC.0000048757.56163.40
6. Betancourt I, Davies HA (2003) J Magn Magn Mater 261:328
7. Chen ZM, Wu YQ, Kramerb MJ, Smith BR, Ma BM, Huang MQ (2004) J Magn Magn Mater 268:105
8. Wu YQ, Kramer MJ, Chen Z, Ma BM, Ping DH, Hono K (2003) IEEE Trans Magn 39:2935
9. Jin ZQ, Okumura H, Zhang Y, Wang HL, Muñoz JS, Hadjipanayis GC (2002) J Magn Magn Mater 248:216
10. Ping DH, Wu YQ, Hono K (2002) J Magn Magn Mater 239:437
11. Wang C, Yan M, Li Q (2007) J Phys D 40:3551
12. Fischer R, Schrefl T, Kronmüller HH, Fidler J (1996) J Magn Magn Mater 153:35
13. Buschow KHJ (1991) In: Long GJ, Grandjean F (eds) Supermagnet, hard magnetic materials. Kluwer Academic Publishers, Dordrecht
14. Hadjipanayis GC, Withanawasam L, Krause RF (1995) IEEE Trans Magn 31:3596
15. Wu YQ, Ping DH, Hono K, Hamano M, Inoue A (2000) J Appl Phys 87:8658
16. Belorizky E, Fremy MA, Gavigan JP, Givord D, Li HS (1987) J Appl Phys 61:3971
17. Sinnema S, Radwanski RJ, Franse JJM, Mooij DB, Buschow KHJ (1984) J Magn Magn Mater 44:333
18. Zhang WY, Yan AR, Zhang HW, Shen BG (2001) J Alloys Compd 315:174